

Simultaneous phase and size control of upconversion nanocrystals through lanthanide doping

Feng Wang¹, Yu Han², Chin Seong Lim³, Yunhao Lu⁴, Juan Wang¹, Jun Xu⁵, Hongyu Chen⁵, Chun Zhang^{1,4}, Minghui Hong^{3,6} & Xiaogang Liu¹

Doping is a widely applied technological process in materials science that involves incorporating atoms or ions of appropriate elements into host lattices to yield hybrid materials with desirable properties and functions. For nanocrystalline materials, doping is of fundamental importance in stabilizing a specific crystallographic phase¹, modifying electronic properties^{2–4}, modulating magnetism⁵ as well as tuning emission properties^{6–9}. Here we describe a material system in which doping influences the growth process to give simultaneous control over the crystallographic phase, size and optical emission properties of the resulting nanocrystals. We show that NaYF₄ nanocrystals can be rationally tuned in size (down to ten nanometres), phase (cubic or hexagonal) and upconversion^{10–12} emission colour (green to blue) through use of trivalent lanthanide dopant ions introduced at precisely defined concentrations. We use first-principles calculations to confirm that the influence of lanthanide doping on crystal phase and size arises from a strong dependence on the size and dipole polarizability of the substitutional dopant ion. Our results suggest that the doping-induced structural and size transition, demonstrated here in NaYF₄ upconversion nanocrystals, could be extended to other lanthanide-doped nanocrystal systems for applications ranging from luminescent biological labels¹² to volumetric three-dimensional displays¹³.

Upconversion nanocrystals are luminescent nanomaterials that convert a near-infrared excitation into a visible emission through lanthanide doping^{10,11}. Compared to organic fluorophores and semi-conducting nanocrystals, upconversion nanocrystals offer high photochemical stability, sharp emission bandwidths, and large anti-Stokes shifts (up to 500 nm) that separate discrete emission peaks from the infrared excitation. Along with the remarkable light penetration depth and the absence of autofluorescence in biological specimens under infrared excitation, these upconversion nanocrystals are ideal for use as luminescent probes in biological labelling and imaging technology. Despite recent progress in nanocrystal synthesis, it has been challenging to prepare small-sized nanocrystals (sub-20 nm) that emit strong upconversion luminescence on infrared excitation¹². Conventional techniques for controlling the crystallization of nanocrystals with well-defined crystal phase and size generally impose stringent control over a set of experimental variables, such as nature of solvent, temperature, reaction time and concentration of metal precursors^{14–26}. For example, hexagonal phase NaYF₄, which offers about an order-of-magnitude enhancement of upconversion efficiency relative to its cubic phase counterpart, typically exists in bulk materials and large-sized particles²⁶. As the physical dimension of the particle is reduced, high surface tension triggers phase transformation from anisotropic (hexagonal) to isotropic (cubic)²⁷, resulting in a significant decrease of upconversion luminescence. Sufficiently high reaction temperatures

(~300 °C) and prolonged heat treatment (up to several days) can lead to the pure hexagonal form of NaYF₄, but these processes are generally associated with significant particle aggregation or enlarged crystal size. Although sub-20-nm hexagonal-phase NaYF₄ nanocrystals have been synthesized in organic solvents²⁶, the synthesis requires air-sensitive, toxic organometallic precursors and hazardous coordinating solvents, which have become matters of substantial environmental concern. Here we present direct observation and mechanistic investigation of simultaneous phase and size control of upconversion NaYF₄ nanocrystals through lanthanide doping. We find that the lanthanide doping approach results in dramatic shortening of reaction time (down to 2 h) on cubic-to-hexagonal phase transition and a substantial decrease in the reaction temperature (down to 230 °C) needed for preparing ultra-small (10 nm) hexagonal phase upconversion nanoparticles.

In cubic sodium rare earth (RE) fluoride systems (NaREF₄) containing one type of high-symmetry cation site, fluorite structures (CaF₂) are formed, with the Ca²⁺ sites randomly occupied by Na⁺ and RE³⁺ ions (Fig. 1a). In contrast, the crystal structure of hexagonal phase NaREF₄ consists of an ordered array of F⁻ ions with two types of relatively low-symmetry cation sites selectively occupied by Na⁺ and RE³⁺ ions (Fig. 1b), resulting in significant electron cloud distortion of the cations to accommodate the structural change. Importantly, light lanthanides with large ionic radii exhibit a high tendency towards electron cloud distortion owing to increased dipole polarizability, and thus favour the hexagonal structures (Fig. 1c). We reasoned that doping of lanthanide ions with a size larger than Y³⁺ ($r = 1.159 \text{ \AA}$)²⁸ in NaYF₄ host lattices should dominate the formation of pure hexagonal-phase NaYF₄ nanocrystals.

To validate our hypothesis, Gd³⁺ ions ($r = 1.193 \text{ \AA}$)²⁸ at different doping levels were used to induce phase transformation in upconversion NaYF₄:Yb/Er nanocrystals. We chose NaYF₄:Yb/Er nanocrystals because of their well-established efficient upconversion luminescence and well developed synthetic methods¹⁹. All samples were first examined by X-ray powder diffraction (Fig. 1d). Without the Gd³⁺ ions added, the X-ray diffraction pattern of NaYF₄:Yb/Er (18/2 mol%) samples can be indexed as a mixture of the cubic (JCPDS file number 77-2042) and hexagonal (JCPDS file number 16-0334) phases of NaYF₄. On doping with increased Gd³⁺ concentrations, the transformation from cubic to hexagonal in these samples is evident. The pure hexagonal phase of NaYF₄ was obtained as the Gd³⁺ ion concentration reached 30 mol%. Notably, the cubic-to-hexagonal phase conversion is complete after heating at 200 °C for only 2 h, much less than the 20 h required for a complete phase transformation without the Gd³⁺ dopant. With further increase in Gd³⁺ ion concentration, no extra diffraction peaks were observed, indicating the formation of a homogeneous Y-Gd solid solution. This result can

¹Department of Chemistry, National University of Singapore, 117543, Singapore. ²Membrane Research Centre, Division of Chemical and Life Science and Engineering, King Abdullah University of Science and Technology, Thuwal 23955-6900, Saudi Arabia. ³Optical Materials and Systems Division, Data Storage Institute, A*STAR, 117608, Singapore. ⁴Department of Physics, National University of Singapore, 117543, Singapore. ⁵Division of Chemistry and Biological Chemistry, Nanyang Technological University, 637371 Singapore. ⁶Department of Electrical and Computer Engineering, National University of Singapore, 117543 Singapore.

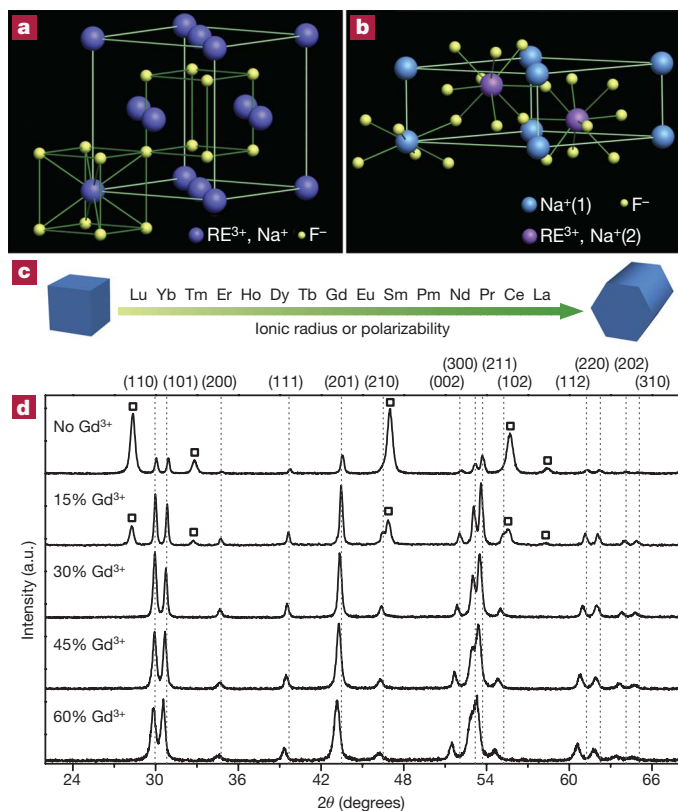


Figure 1 | Phase transformation in NaREF₄ structures by lanthanide doping. **a, b**, Schematic presentation of cubic- and hexagonal-phase NaREF₄ structures, respectively. In the cubic phase, equal numbers of F⁻ cubes contain cations and vacancies. In the hexagonal phase, an ordered array of F⁻ ions offers two types of cation sites: one occupied by Na⁺ and the other occupied randomly by RE³⁺ and Na⁺. **c**, General trend of phase transition from cubic to hexagonal as a function of ionic radius (or polarizability) of the lanthanide dopant ions. **d**, X-ray powder diffraction patterns of the NaYF₄:Yb/Er (18/2 mol%) nanocrystals obtained after heating for 2 h at 200 °C in the presence of 0, 15, 30, 45 and 60 mol% Gd³⁺ dopant ions, respectively. Diffraction peaks corresponding to cubic NaYF₄ are marked with square boxes. A gradual decrease in diffraction peak intensities for cubic phase is observed as a function of increased Gd³⁺ dopant content.

be attributed to the small structural difference between the hexagonal phase NaYF₄ and NaGdF₄. They adopt the same space group (*P6₃/m*) with similar unit-cell parameters ($a = 5.96 \text{ \AA}$, $c = 3.53 \text{ \AA}$ for NaYF₄ and $a = 6.02 \text{ \AA}$, $c = 3.60 \text{ \AA}$ for NaGdF₄). The peak shifts towards lower diffraction angles in the X-ray powder diffraction patterns as a function of the Gd³⁺ ion concentration arise as a result of expansion in unit-cell volume owing to the substitution of Y³⁺ ions by larger Gd³⁺ ions in the host lattice. Importantly, we also observed that the diffraction peaks broaden with increasing Gd³⁺ dopant content, indicating a reduction of the average crystallite size.

To shed more light on the effect of lanthanide doping, we performed first principles calculations based on density functional theory (DFT) for ground-state geometry and formation energy of NaYF₄ and NaGdF₄ nanocrystals in both cubic and hexagonal phases (Supplementary Fig. 1). The DFT calculations include the generalized gradient approximation²⁹, using a plane wave basis (kinetic energy cut-off 400 eV) and projector augmented-wave pseudo potential³⁰. The formation energy is defined as the energy difference per unit cell between the nanocrystal and isolated atoms. In cubic phase, the formation energy per atom decreases by about 0.07 eV when Y³⁺ is replaced by Gd³⁺, representing the fact that NaYF₄ is more energetically stable than NaGdF₄ in cubic phase. In contrast, the formation energy per atom in hexagonal phase increases by about 0.07 eV when Y³⁺ is replaced by Gd³⁺, indicating that NaGdF₄ is more energetically

stable than NaYF₄ in hexagonal phase. Our calculations are consistent with our experimental observations showing that an increase of the Gd³⁺ dopant content in the NaYF₄ host favours the formation of hexagonal phase nanocrystals.

We further studied the crystal structure and size of NaYF₄:Yb/Er (18/2 mol%) samples doped with Gd³⁺ ions at different concentrations (0–60 mol%) using transmission electron microscopy (TEM) (Fig. 2). Without deliberately added Gd³⁺ ions, the TEM image of the NaYF₄:Yb/Er (18/2 mol%) sample prepared in an aqueous solvent for 2 h shows two distinct particle morphologies that include small nanocubes and large nanorods (Fig. 2a), well consistent with the presence of two phases observed by X-ray powder diffraction. TEM images of samples obtained after 5 and 10 h of reactions still show the formation of mixed nanorods and nanocubes (Fig. 2b and c). High-resolution TEM analysis reveals that the small nanocubes are cubic phase NaYF₄ (Fig. 2d). We therefore concluded the large nanorods to be hexagonal-phase NaYF₄ and we further confirmed this by electron diffraction study (Fig. 2e). However, in the presence of Gd³⁺ dopant ions (30 mol%), the cubic-to-hexagonal phase conversion is clearly complete after only 2 h under identical reaction conditions (Fig. 2f). The dramatic shortening of reaction time on phase transformation was further confirmed by repeated doping experiments with 45 mol% and 60 mol% of Gd³⁺. In all cases, the complete conversion of cubic to hexagonal phase occurred after 2 h, resulting in formation of highly uniform nanorods (Fig. 2g and h). With increasing Gd³⁺ dopant concentration (30–60 mol%), nanorods with gradually decreased dimensions are formed (Fig. 2f–h), which is consistent with a previous report in the case of Eu³⁺ doping²². We determined the nanorods with a Gd³⁺ content of 60 mol% to be highly crystalline hexagonal phase using high-resolution TEM (Fig. 2i). Lattice fringes associated with (001) planes (d -spacing of 0.36 nm) appear along the nanorods, indicating that the nanorods grow along the c axis (Supplementary Fig. 2). Compositional analysis of an individual nanorod by energy-dispersive X-ray spectroscopy reveals the presence of the doped elemental Yb, Er and Gd (Supplementary Fig. 2).

The size evolution of NaYF₄:Yb/Er nanocrystals can be partly attributed to the strong effect of the Gd³⁺ dopant ion on crystal growth rate through surface charge modification. Our DFT calculation shows that the electron charge density of the crystal surface increases after a Gd³⁺ ion substitutes the Y³⁺ ion in the crystal lattice. The change of electron charge density on the surface of the small-sized nanocrystals can substantially slow the diffusion of negatively charged F⁻ ions to the surface, owing to an increase in charge repulsion, resulting in a tunable reduction of the NaYF₄ nanocrystal size (Fig. 2j).

To verify the phase and size control mechanism of this doping approach, larger lanthanide ions Sm³⁺ ($r = 1.219 \text{ \AA}$)²⁸ and Nd³⁺ ($r = 1.249 \text{ \AA}$)²⁸ were each doped into the NaYF₄:Yb/Er nanocrystals at a dopant concentration of 30 mol%. Both samples were found to crystallize in pure hexagonal phase with rod-like morphology (Supplementary Fig. 3). The larger Sm³⁺ and Nd³⁺ ions resulted in the formation of smaller nanorods than did the Gd³⁺ ion under identical reaction conditions. These results further confirm that the size and dipole polarizability of the lanthanide ion dominate the phase and size evolution of the NaYF₄ nanocrystals. We note that in the presence of a dopant ion (for example, La³⁺, $r = 1.300 \text{ \AA}$)²⁸ with a significantly larger ionic size than the Y³⁺ ion, hexagonal phase NaYF₄ nanorods were not obtained (Supplementary Fig. 3). This can be ascribed to the large disparity in size between the La³⁺ and Y³⁺ ions, which leads to the formation of stable LaF₃ phase (Supplementary Fig. 3) rather than a homogenous La–Y solid solution.

Although several lanthanide dopant ions have been shown to control the crystal phase and size of upconversion NaYF₄:Yb/Er nanocrystals, only the Gd³⁺ dopant ion is shown to favour the upconversion luminescence. Photoluminescence investigation revealed that the NaYF₄:Yb/Er nanocrystals doped with Sm³⁺ or Nd³⁺ ions (30 mol%)

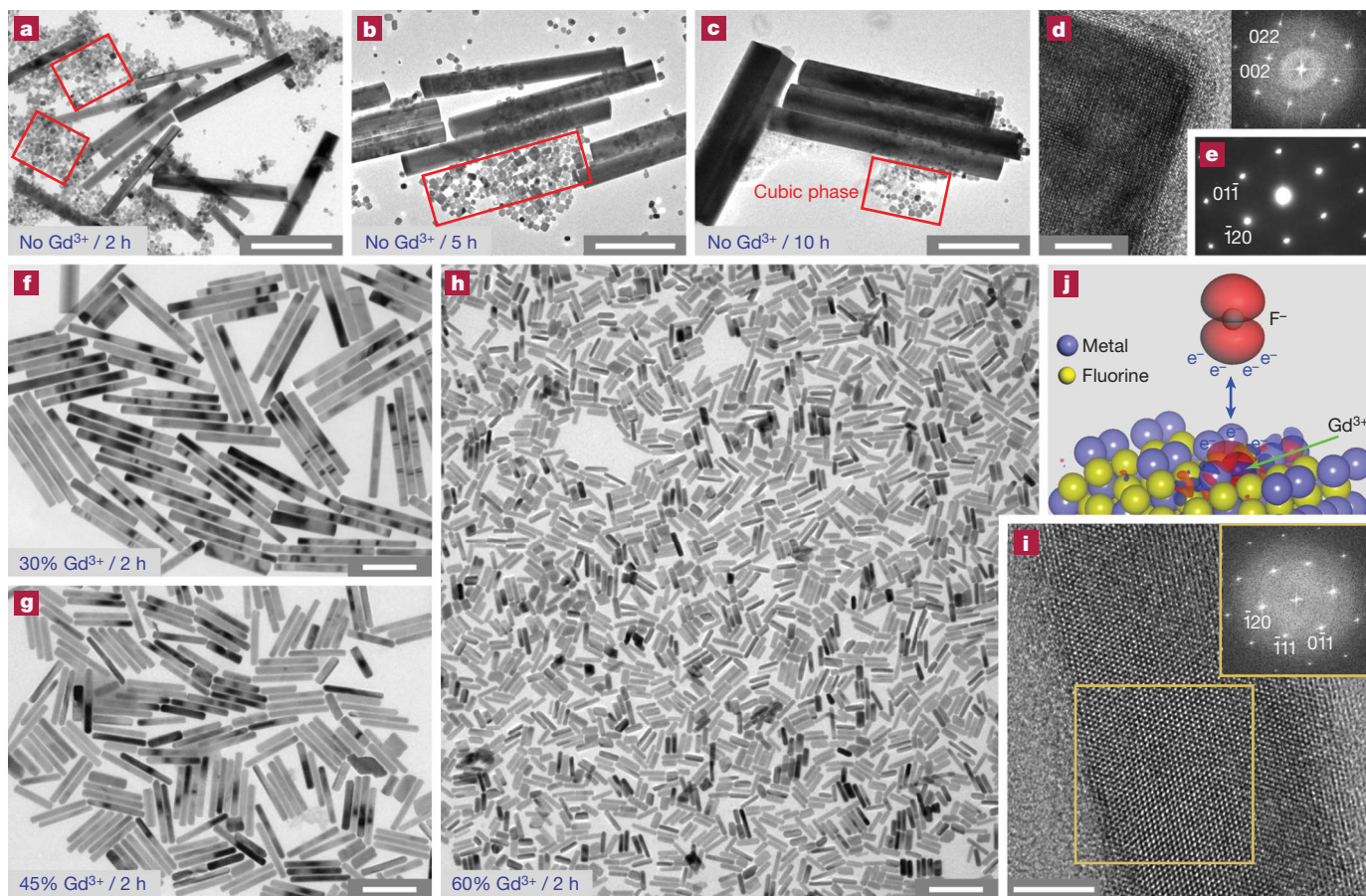


Figure 2 | TEM characterization of NaYF₄:Yb/Er (18/2 mol%) nanocrystals doped with various concentrations of Gd³⁺ ions. **a–c**, TEM images of NaYF₄:Yb/Er (18/2 mol%) products obtained after heating for 2, 5 and 10 h in the absence of Gd³⁺ dopant ions. Formation of the cubic phase products is partially marked by red squares. **d**, High-resolution TEM image taken in [100] incidence and the corresponding Fourier-transform diffractogram (inset) of a nanocube in the mixture shown in **a**, indicating the cubic phase of the nanocube. **e**, Selected area electron diffraction pattern taken in [211] incidence of a nanorod in the mixture shown in **a**, indicating formation of the hexagonal-phase nanorod. **f–h**, TEM images of the

NaYF₄:Yb/Er (18/2 mol%) products obtained after heating for 2 h in the presence of 30, 45 and 60 mol% Gd³⁺ dopant ions, respectively. **i**, High-resolution TEM image taken in [211] incidence and the corresponding Fourier-transform diffractogram (inset) of a nanorod shown in **h**, indicating the hexagonal phase of the nanorod. The yellow square on the rod indicates the area selected for Fourier transformation. **j**, DFT calculation showing the change of surface charge density caused by replacing the Y³⁺ in the host lattice with a Gd³⁺ ion. The red shading around the Gd³⁺ ion denotes the increased negative charges upon ion exchange. Scale bars are 500 nm for panels **a–c**, 200 nm for panels **f–h** and 5 nm for panels **d** and **i**.

do not emit visible upconversion luminescence. In contrast, the presence of Gd³⁺ dopant ions at a broad concentration range has no quenching effect on upconversion luminescence (Fig. 3a). This difference is probably due to quenching of the excitation energy through efficient energy transfer from Yb³⁺ and Er³⁺ to ⁶F₁ manifolds of Sm³⁺ and ⁴I₁ manifolds of Nd³⁺, respectively (Fig. 3b and c). In Gd³⁺ doped systems, the lowest excited level (⁶P_{7/2}) of Gd³⁺ is situated in the ultraviolet region (Fig. 3d), which is far higher than most excited levels of Yb³⁺ and Er³⁺ involved in the upconversion processes. Thus, excitation energy loss through energy transfer from Yb³⁺ and Er³⁺ to 4f levels of Gd³⁺ can be avoided. We also note that the emission intensity of NaYF₄:Yb/Er/Gd nanocrystals increases with increase in Gd³⁺ concentration to 15 mol% and then exhibits a gradual decrease upon further increase in Gd³⁺ dopant content. The initial increase in emission intensity can be associated with the increase in relative amount of hexagonal phase in the crystal structure. The subsequent decrease in emission intensity is primarily attributed to the reduction in crystal size. Smaller nanocrystals tend to have increased surface quenching sites and thus suppress upconversion luminescence by enhanced nonradiative energy transfer processes of the luminescent lanthanide ions.

To test the doping-induced crystal phase and size tuning further, we carried out the synthesis of NaYF₄:Yb/Er upconversion nanoparticles by Gd³⁺ doping in organic solvents at different temperatures.

Without the Gd³⁺ ion added, a substantially high temperature of 300 °C is needed to generate hexagonal-phase nanoparticles with an average diameter of 25 nm. On increasing Gd³⁺ dopant concentration, the size of nanoparticles can be tuned down to 10 nm (Supplementary Fig. 5). More importantly, we found that the Gd³⁺ doping can lead to a significant decrease in the reaction temperature (down to 230 °C) required for preparing hexagonal phase nanoparticles (Supplementary Fig. 6). We found that the large decrease in reaction temperature had almost no effect on the size and morphology of NaYF₄ nanoparticles. In contrast, the reaction at 230 °C in the absence of Gd³⁺ dopant ions yielded mostly polydisperse NaF crystals rather than monodisperse NaYF₄ nanoparticles. The results further confirm that the doping of Gd³⁺ promotes cubic-to-hexagonal phase transformation in NaYF₄ nanocrystals.

The successful preparation of ultra-small nanoparticles with strong upconversion luminescence by lanthanide doping suggests that it is now possible to synthesize upconversion nanocrystals with simultaneous control over crystal phase, size and emission colours through the control of different combinations of lanthanide dopants at precisely defined concentrations. For example, small-sized NaYF₄ upconversion nanoparticles that emit tunable visible colours were readily synthesized by rational doping of Yb³⁺, Er³⁺, Gd³⁺ and Tm³⁺ ions at different concentrations. The addition of a second emitter (Tm³⁺) at a trace concentration of 0.2 mol% had a negligible effect

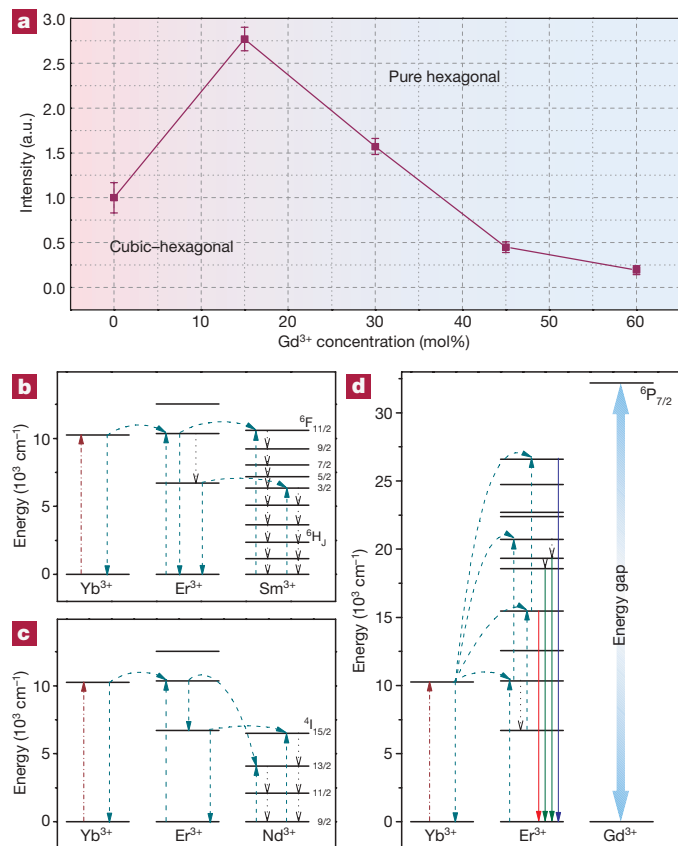


Figure 3 | Photoluminescence studies of NaYF₄:Yb/Er (18/2 mol%) nanocrystals with varying dopant concentration of Gd³⁺. **a**, Upconversion emission intensity versus dopant concentration of Gd³⁺ (0–60 mol%). The emission intensities were calculated by integrating the spectral intensity of the emission spectra over wavelength in the range 400–700 nm. Error bars shown represent the standard deviations from three repeated measurements. **b–d**, Proposed energy transfer mechanisms under 980-nm diode laser excitation in NaYF₄:Yb/Er nanocrystals doped with Sm³⁺, Nd³⁺, and Gd³⁺, respectively. The dashed-dotted, dashed, dotted, and full arrows represent photon excitation, energy transfer, multiphonon relaxation, and emission processes, respectively. The ^{2S+1}L_J notations used to label the *f* levels refer to spin (*S*), orbital (*L*) and angular (*J*) momentum quantum numbers, respectively, according to the Russel–Saunders notation.

on nanocrystal phase and size, but induced colour change markedly from green to blue (Fig. 4a and b). Owing to their small feature size and ease of dispersion, these nanoparticles can readily be incorporated in polydimethylsiloxane (PDMS) monoliths to construct volumetric three-dimensional (3D) displays (Fig. 4c and d), presenting unique interface applications for 3D image visualization. In contrast to conventional two-frequency resonant absorption techniques reliant on excitation of two near-infrared laser beams that intersect inside a glass-like matrix¹³, this single-beam design offers a simple system configuration and solves the problems of ghost voxels and alignment between beams.

In stark contrast to conventional synthetic techniques that require stringent control over several experimental variables for controlling crystallite size and phase, the lanthanide doping approach presented here requires modification of only a single variable (dopant concentration), while enabling tremendous improvements in our ability to control the formation of upconversion nanocrystals with small feature size and desirable optical properties. These findings are important not only for understanding lanthanide-doping-mediated crystal growth process, but also for providing a convenient route for facile synthesis of ultra-small hexagonal phase NaYF₄ upconversion nanocrystals without the need for toxic organometallic precursors and hazardous coordinating solvents. As an added benefit, the use of

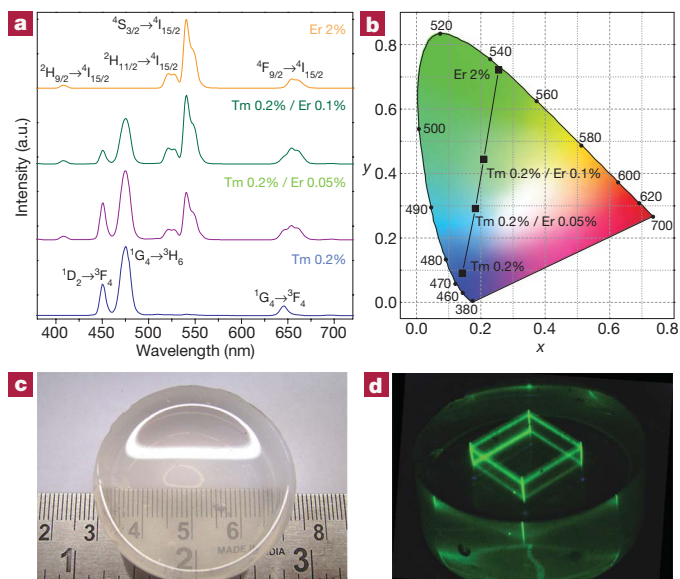


Figure 4 | Photoluminescence studies of NaYF₄ nanocrystals dispersed in solutions and embedded in PDMS composite materials. **a**, Room-temperature (25 °C) upconversion emission spectra of cyclohexane solutions comprising NaYF₄:Yb/Er/Gd (18/2/5 mol%), NaYF₄:Yb/Tm/Er/Gd (20/0.2/0.1/5 mol%), NaYF₄:Yb/Tm/Er/Gd (20/0.2/0.05/5 mol%), and NaYF₄:Yb/Tm/Gd (20/0.2/5 mol%) nanoparticles, respectively. **b**, Corresponding Commission Internationale de l'Éclairage (CIE) chromaticity coordinates of the multicolour emissions from the samples shown in **a**. **c**, Photograph showing physical dimension and transparency of a PDMS sample composed of 0.1 wt% of NaYF₄:Yb/Er/Gd (18/2/5 mol%) nanoparticles. **d**, Luminescent image of a 3D structure generated in the PDMS sample via computer-controlled near-infrared laser scanning.

paramagnetic Gd³⁺ dopant ions provides the nanocrystals with a second imaging capability as magnetic resonance imaging probes¹⁵.

METHODS SUMMARY

Nanocrystal synthesis. We synthesized lanthanide-doped NaYF₄ nanorods and nanoparticles capped with oleic acid using the methods of ref. 19 and ref. 23, respectively. Additional experimental details are provided in the Supplementary Information.

Preparation of the nanoparticle/PDMS composite materials. A 10:1:1 (vol:vol:vol) mixture of SYLGARD silicone elastomer 184, the curing agent (Dow Corning Corp.), and a cyclohexane solution containing upconversion nanoparticles (1 wt%) were thoroughly mixed in a glass container and aged overnight before heat treatment at 81 °C for 1 h. The composite materials with different types of nanoparticles can easily be cut into rectangular bars.

Volumetric 3D display. A 980-nm diode laser operating at 2,000 mW was directed into a fast scanning X-Y galvanometer with an F-theta lens (focal length of 198 mm) to focus the laser beam. A dynamic beam expander was attached to the galvanometer to control the Z position of the laser beam at a range of ±7 mm. The scanning of the laser beam was controlled through CyberLease scanning software from IDI Laser. A 3D cube structure was then drawn and imported into CyberLease to generate a 3D scanning path for the laser beam. During the writing process, the laser beam was scanned across the sample by altering the X-Y mirror of the galvanometer while the height of the laser focal point was changed by changing the expanded beam size. The laser power was attenuated to 27 mW and the scanning speed was set at 2 mm s⁻¹.

Received 25 June; accepted 15 December 2009.

- Feng, X. *et al.* Converting ceria polyhedral nanoparticles into single-crystal nanospheres. *Science* **312**, 1504–1508 (2006).
- Alivisatos, A. P. Semiconductor clusters, nanocrystals, and quantum dots. *Science* **271**, 933–937 (1996).
- Norris, D. J., Yao, N., Charnock, F. T. & Kennedy, T. A. High-quality manganese-doped ZnSe nanocrystals. *Nano Lett.* **1**, 3–7 (2001).
- Yang, Y., Chen, O., Angerhofer, A. & Cao, Y. C. Radial-position-controlled doping in CdS/ZnS core/shell nanocrystals. *J. Am. Chem. Soc.* **128**, 12428–12429 (2006).
- Wernsdorfer, W. *et al.* Macroscopic quantum tunneling of magnetization of single ferrimagnetic nanoparticles of barium ferrite. *Phys. Rev. Lett.* **79**, 4014–4017 (1997).

- Heer, S., Kömpe, K., Güdel, H.-U. & Haase, M. Highly efficient multicolour upconversion emission in transparent colloids of lanthanide-doped NaYF₄ nanocrystals. *Adv. Mater.* **16**, 2102–2105 (2004).
- Sivakumar, S., van Veggel, F. C. J. M. & Raudsepp, M. Bright white light through up-conversion of a single NIR source from sol-gel-derived thin film made with Ln³⁺-doped LaF₃ nanoparticles. *J. Am. Chem. Soc.* **127**, 12464–12465 (2005).
- Ehlert, O., Thomann, R., Darbandi, M. & Nann, T. A. Four-color colloidal multiplexing nanoparticle system. *ACS Nano* **2**, 120–124 (2008).
- Wang, F. & Liu, X. Upconversion multicolor fine-tuning: visible to near-infrared emission from lanthanide-doped NaYF₄ nanoparticles. *J. Am. Chem. Soc.* **130**, 5642–5643 (2008).
- Auzel, F. Upconversion and anti-stokes processes with f and d ions in solids. *Chem. Rev.* **104**, 139–173 (2004).
- Suyver, J. F. et al. Novel materials doped with trivalent lanthanides and transition metal ions showing near-infrared to visible photon upconversion. *Opt. Mater.* **27**, 1111–1130 (2005).
- Wang, F. & Liu, X. Recent advances in the chemistry of lanthanide-doped upconversion nanocrystals. *Chem. Soc. Rev.* **38**, 976–989 (2009).
- Downing, E., Hesselink, L., Ralston, J. & Macfarlane, R. A three-color, solid-state, three-dimensional display. *Science* **273**, 1185–1189 (1996).
- Liu, C., Wang, H., Zhang, X. & Chen, D. Morphology- and phase-controlled synthesis of monodisperse lanthanide-doped NaGdF₄ nanocrystals with multicolor photoluminescence. *J. Mater. Chem.* **19**, 489–496 (2009).
- Park, Y. I. et al. Nonblinking and nonbleaching upconverting nanoparticles as an optical imaging nanoprobe and T1 magnetic resonance imaging contrast agent. *Adv. Mater.* **21**, 4467–4471 (2009).
- Lim, B. et al. Pd-Pt bimetallic nanodendrites with high activity for oxygen reduction. *Science* **324**, 1302–1305 (2009).
- Sun, S., Murray, C. B., Weller, D., Folks, L. & Moser, A. Monodisperse FePt nanoparticles and ferromagnetic FePt nanocrystal superlattices. *Science* **287**, 1989–1992 (2000).
- Tang, Z., Zhang, Z., Wang, Y., Glotzer, S. C. & Kotov, N. A. Self-assembly of CdTe nanocrystals into free-floating sheets. *Science* **314**, 274–278 (2006).
- Wang, X., Zhuang, J., Peng, Q. & Li, Y. A general strategy for nanocrystal synthesis. *Nature* **437**, 121–124 (2005).
- Cademartiri, L. et al. Multigram scale, solventless and diffusion-controlled route to highly monodisperse PbS nanocrystals. *J. Phys. Chem. B* **110**, 671–673 (2006).
- Chen, Y., Kim, M., Lian, G., Johnson, M. B. & Peng, X. Side reactions in controlling the quality, yield, and stability of high quality colloidal nanocrystals. *J. Am. Chem. Soc.* **127**, 13331–13337 (2005).
- Wang, L. & Li, Y. Controlled synthesis and luminescence of lanthanide doped NaYF₄ nanocrystals. *Chem. Mater.* **19**, 727–734 (2007).
- Li, Z., Zhang, Y. & Jiang, J. Multicolor core/shell-structured upconversion fluorescent nanoparticles. *Adv. Mater.* **20**, 4765–4769 (2008).
- Mai, H. et al. High-quality sodium rare-earth fluoride nanocrystals: controlled synthesis and optical properties. *J. Am. Chem. Soc.* **128**, 6426–6436 (2006).
- Boyer, J. C., Vetrone, F., Cuccia, L. A. & Capobianco, J. A. Synthesis of colloidal upconverting NaYF₄ nanocrystals doped with Er³⁺, Yb³⁺ and Tm³⁺, Yb³⁺ via thermal decomposition of lanthanide trifluoroacetate precursors. *J. Am. Chem. Soc.* **128**, 7444–7445 (2006).
- Yi, G. S. & Chow, G. M. Synthesis of hexagonal-phase NaYF₄:Yb,Er and NaYF₄:Yb,Tm nanocrystals with efficient up-conversion fluorescence. *Adv. Funct. Mater.* **16**, 2324–2329 (2006).
- Ayyub, P., Palkar, V. R., Chattopadhyay, S. & Multani, M. Effect of crystal size reduction on lattice symmetry and cooperative properties. *Phys. Rev. B* **51**, 6135–6138 (1995).
- Shannon, R. D. Revised effective ionic radii and systematic studies of interatomic distances in halides and chalcogenides. *Acta Crystallogr. A* **32**, 751–767 (1976).
- Perdew, J. P., Burke, K. & Ernzerhof, M. Generalized gradient approximation made simple. *Phys. Rev. Lett.* **77**, 3865–3868 (1996).
- Bloch, P. E. Projector augmented-wave method. *Phys. Rev. B* **50**, 17953–17979 (1994).

Supplementary Information is linked to the online version of the paper at www.nature.com/nature.

Acknowledgements We thank G. A. Ozin, X. Chen, F. Stellacci, C. Yan, Y. Xia, L. Cademartiri, T. Nann, Y. Li and Y. C. Cao for discussions. This study was supported in part by the National University of Singapore (NUS), the Ministry of Education of Singapore, the Singapore-MIT Alliance, and the Agency for Science, Technology and Research (A*STAR). X.L. is grateful to the NUS for a Young Investigator Award.

Author Contributions F.W. and X.L. conceived the experiments and wrote the paper. F.W. and J.W. were primarily responsible for the experiments. Y.H., J.X. and H.C. performed the TEM characterization. C.S.L. and M.H. contributed to the volumetric 3D display studies. Y.L. and C.Z. performed theoretical calculations. All authors contributed to the analysis of this manuscript.

Author Information Reprints and permissions information is available at www.nature.com/reprints. The authors declare no competing financial interests. Correspondence and requests for materials should be addressed to X.L. (chmlx@nus.edu.sg).